Empirical Analysis of Multipath and Non-Line-of-Sight Errors on Receiver Measurements in an Urban Environment

Matt Peretic, *The MITRE Corporation*
Jon Christie, *The MITRE Corporation*
Russell Gilabert, *NASA Langley Research Center*
Dr. Johnson Carroll, *The MITRE Corporation*
Dr. Julian Gutierrez, *NASA Langley Research Center*
Dr. Andrew Moore, *NASA Langley Research Center*
Dr. Evan T. Dill, *NASA Langley Research Center*

ABSTRACT

Signals from global navigation satellite systems (GNSS) are prone to multipath interference and non-line-of-sight (NLOS) reception in urban environments. Buildings surrounding a receiver are liable to block the line-of-sight (LOS) to GNSS satellites and reflect copies of GNSS signals, causing much greater errors in the pseudorange measurements compared to open-sky environments. Such pseudorange errors can lead to navigation solution inaccuracies that can introduce considerable mission risk, particularly if the errors are comparable to or greater than the distance between buildings (canyon width). This study analyzes statistical trends in pseudorange measurements from two commercial GNSS receivers onboard a vehicle traveling through a dense urban canyon. Data collection included multiple laps around the same city blocks to average out the influence of instantaneous satellite geometry. A 3D digital elevation map and ray-casting methods were used to classify whether measurements were LOS or NLOS. To analyze the statistical behavior of pseudorange errors attributed to multipath interference and NLOS reception for each receiver, separate histograms were generated from the errors on the LOS measurements and the errors on the NLOS measurements. The primary findings include a quantitative comparison of the difference in the weight of the tails in the statistical distribution of the errors on the NLOS measurements and the study of one particular case where the statistical distribution of the pseudorange errors from individual satellites have asymmetric tails which appear to mirror each other. This empirical analysis can inform what statistical performance may or may not be consistent across receivers in urban environments.

I. INTRODUCTION

From emergency services to emerging business models, there is a growing demand for urban flight operations (Patterson et al., 2021). To ensure safety, prospective missions require rigorous risk assessment built on thorough technical analysis. Navigation risk is a key facet of the mission risk, particularly in advanced air mobility (AAM) and urban air mobility (UAM) contexts where the mission is expected to be conducted between in canyon-like corridors of buildings. These deep urban environments offer particular challenges to global navigation satellite system (GNSS)-based navigation, where buildings may reflect copies of GNSS signals with little power loss and may simultaneously block the line-of-sight (LOS) to GNSS satellites. Such signal propagation effects can impact the GNSS receiver's pseudorange measurements to the satellites if they introduce errors that behave differently than the fundamental assumptions on which the receiver and the mission's GNSS integrity metrics were designed. If these differences are significant enough, the receiver and the existing risk assessment methods could produce hazardously misleading information. This work seeks to deepen the body of knowledge on trends in the statistical behavior of pseudorange errors in urban environments.

This paper expands on the authors' previous effort to empirically study multipath interference and non-line-of-sight (NLOS) effects present in urban canyon environments, and their impacts on pseudorange errors. The prior work, (Peretic et al., 2025), presented a methodology to isolate the component of the pseudorange errors due to multipath interference and NLOS effects from observables recorded by a single commercial receiver in an urban environment. This work investigates the performance of

This technical data was produced in part for the U. S. Government under Purchase Order 80NSSC24PB490, and is subject to the Rights in Data-General Clause 52.227-14, Alt. IV (DEC 2007). Approved for Public Release; Distribution Unlimited. Public Release Case Number 25-1850.

two GNSS receivers in a deeper urban canyon environment. The findings in this study include a time-series comparison of the measurements produced by the two receivers, analysis and comparison of histograms characterizing the statistical distribution of the errors caused by multipath interference and NLOS reception in the pseudorange measurements, and an investigation of certain statistical behaviors observed on individual satellites.

II. BACKGROUND

Multipath interference and NLOS reception are signal propagation effects that arise when a reflection of a signal arrives at a receiver (Betz, 2015, Chapter 22). If the receiver still receives the LOS signal alongside a reflected copy or copies of that signal, the reflected copy or copies are called multipath interference (McGraw et al., 2021). If the LOS signal is not present and only a reflected copy or copies arrive, it is called NLOS reception (McGraw et al., 2021). Since GNSS receivers typically measure time of flight (ToF), multipath interference and NLOS reception can introduce delayed copies of the signal, which distort the receiver's correlation results and lead to errors in the ToF measurements. The receiver typically then formulates pseudorange measurements from the ToF measurements and employs the pseudorange measurements in computing the navigation solution.

Understanding the statistical behavior of these errors is essential for both developing navigation algorithms robust to these effects and in assessing receiver integrity in the presence of these effects (Zhu et al., 2018). The standard Kalman filter, which a receiver may employ in the navigation stage of its processing, is built on the assumption that the statistical behavior of the pseudorange errors follow a zero-mean Gaussian model. When these assumptions are violated, the filter can produce misleading information (McGraw et al., 2021). Kalman filter variants have been proposed which do not have a zero-mean Gaussian assumption, but the measurements which they process need to fit the statistical assumptions that they do employ. If the true behavior of the errors violate the statistical model, as with the zero-mean Gaussian assumption, the filter's results can be misleading. If the error model is too conservative and does not closely fit the true behavior of the errors, the navigation filter's results will have significant uncertainty, which may not be acceptable for the narrow corridors of AAM/UAM missions.

Analytical techniques, like the well-known multipath error envelope, characterize the limits of a receiver's pseudorange errors from the tracking loop stage given by a) the tracking loop's discriminator and tap spacing and b) the relative power between the true signal and a delayed copy of the signal (Betz, 2015, Chapter 22). This can be extended to NLOS effects by choosing one of the copies of the NLOS signal as the "primary" copy and adding the extra distance that the signal copy traveled as a bias to the envelope. However, the multipath error envelope model requires knowledge of the number of copies of the signal and their relative powers. The multipath error envelope would have to be computed under each set of multipath and NLOS effects expected, and then combined based on their expected rates of occurrence. This analysis can reveal the limits of the pseudorange errors, but additional modeling would be required to model the statistical behavior of the errors.

As surveyed in (Peretic et al., 2025), empirical studies of the distribution of pseudorange errors such as (Matera et al., 2019), (Chen, 2018), and (Wang et al., 2018) study the behavior of the measurements that a specific receiver produced in an urban environment. The work of (Matera et al., 2019) introduces a methodology for post-processing recorded observables from a receiver to isolate the component of the pseudorange error due to multipath interference and NLOS reception. Subsequent work in (Peretic et al., 2025) introduced ray-based satellite visibility modeling to this methodology. This enables the component of pseudorange error due to the receiver's clock bias to be estimated and removed using known LOS measurements, and enables the statistical distribution of the errors of LOS and NLOS measurements to be studied independently. In the dataset studied in the prior work, the LOS measurements showed a near-zero mean, nearly symmetric distribution, while the NLOS measurements showed a non-zero mean, asymmetric, heavy-tailed distribution. The ray-based satellite visibility modeling also enabled another concept to be introduced: quantitative depth and "sidedness" metrics to characterize urban canyons as a function of elevation and azimuth angle from the perspective of the receiver. This enabled a study of how the statistical behavior of the pseudorange errors vary as a function of these urban canyon features, which showed that the tails on the error distributions for the NLOS measurements increased as the canyon depth increased with canyon depth and symmetry.

III. METHODOLOGY

This work will continue to empirically explore the statistical behavior of pseudorange errors in urban environments. To isolate the effects of multipath interference and NLOS reception on pseudorange error, the results in Section V will utilize the methodology detailed in (Peretic et al., 2025) and briefly summarized below; more details can be found in the reference. This methodology estimates and removes all known errors from the receiver's pseudorange measurements except for those due to multipath interference, NLOS reception, and thermal noise. As shown in Figure 1, the methodology begins with four inputs: a test receiver's pseudorange measurements, the true position of the receiver as measured by a separate sensor with a known degree of accuracy, digital elevation map data, and measurements from a stationary reference receiver at a known location which is not expected to experience multipath effects and NLOS reception.

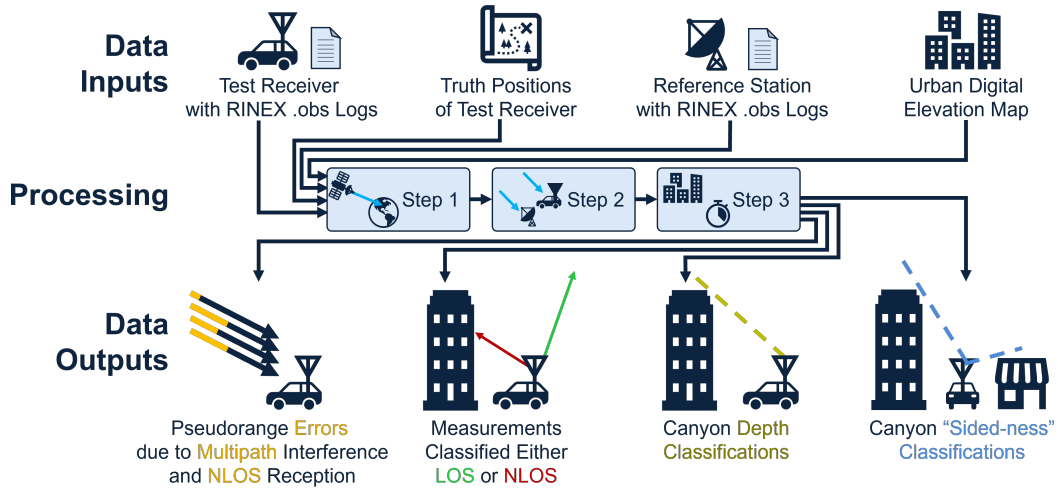

Figure 1: Data inputs and outputs for the pseudorange error isolation methodology.

Figure 2 provides an overview of the methodology's processing steps. The first step of the methodology uses the receiver's known true position to calculate the true range to the satellite, then subtract it from the test receiver's pseudorange measurement. The second step involves performing a single difference between the reference receiver's measurement residuals and the residuals for the test receiver as computed in the previous step. This removes "common mode" errors experienced by multiple receivers, including those from satellite clock and ephemeris, relativistic effects, ionosphere, and troposphere. The final step of the methodology is to estimate and remove the receiver clock bias from the measurements. This is accomplished by taking the least squares solution of the test receiver's LOS measurements with the position component of the solution fixed to the known true position. The resultant time series of clock bias estimates is low-pass filtered to mitigate the noise and multipath effects which are high-frequency with respect to the filter tuning parameters.

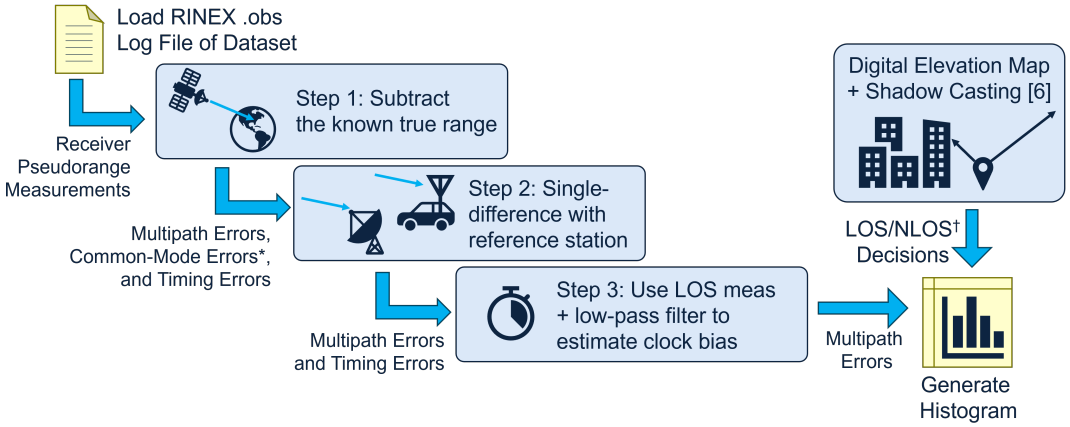

Figure 2: Overview of processing steps for pseudorange error isolation methodology.

In parallel with this methodology, the measurements are classified as LOS or NLOS by propagating the LOS ray and checking for intersection with the terrain model from a digital elevation map. The specific technique employed here, shadow casting, accomplishes this by identifying the minimum height where a satellite becomes visible at all points in the city (Dill et al., 2021). Measurements are classified as LOS or NLOS by looking up the receiver truth position when the measurement was made and checking whether the altitude at that truth position is greater than the minimum height of the shadow map.

This shadow casting methodology is also employed to characterize the urban canyon. For each point on the trajectory, the maximum elevation angle to the top of the terrain as a function of azimuth is modeled from the digital elevation map. This produces two classification labels, one describing canyon depth and one describing the difference in depth between the two

sides. This provides quantitative metrics for comparing urban environments and studying the similarities and differences in the statistical behavior of pseudorange errors between them. This approach is described further in (Peretic et al., 2025).

After processing the measurements with this methodology, the pseudorange error due to multipath effects and NLOS reception is left, and all measurements are marked as LOS or NLOS, with two additional canyon characterization labels.

IV. DATASET DESCRIPTION

The data analyzed in the subsequent section was collected in downtown Boston, Massachusetts, in April 2025. Two test receivers and the truth reference sensor were connected to vehicle-mounted patch antennas and driven through a dense urban canyon region of the city, as shown in Figure 3 and Figure 7. The vehicle drove over the same stretch of road six times in succession over a roughly 90-minute interval in order to reduce the impact of one particular GNSS satellite configuration on the results.

A u-Blox EVK-M8T-0 (henceforth referred to as the u-Blox M8) and a Septentrio Mosaic Go-H (henceforth referred to as the Septentrio Mosaic) served as the test receivers. Both the u-Blox M8 and Septentrio Mosaic recorded multi-GNSS pseudorange measurements on the L1 and L2 frequencies. The u-Blox M8 recorded measurements at 1Hz, while the Septentrio Mosaic recorded measurements at 10Hz. The Septentrio Mosaic's measurements were decimated to match the rate of the u-Blox M8, choosing the measurements nearest to the top of the UTC second. For this study, only the receivers' measurements from the GPS L1 C/A signal were used in the analysis. The Septentrio Mosaic uses two antennas for heading estimation, and subsequent results use the pseudorange measurements that the Septentrio Mosaic collected from the same antenna as the single-antenna u-Blox M8. The antennas used were both the TE Connectivity ANT-GNRM-L125A-series, which are right-hand circular polarized, L1/L2/L5 multi-frequency antennas with an internal low-noise amplifier.

For the truth reference, a u-Blox EVK-F9P-16 ("F9P") recorded position data from the same antenna as the test receiver. The F9P receiver navigated in a multi-constellation, multi-frequency mode using GNSS signals on the L1 and L5 bands. The position estimates produced were post-processed to clamp the altitude to 2m above ground level (accounting for the height of the vehicle), and were manually inspected to ensure that their horizontal accuracy was consistent with the road lane in which the vehicle had driven.

The International GNSS Service (IGS) station WES2, located in Westford, Massachusetts, provided the reference receiver measurements. This station is slightly less than 50km from the data collection area, which satisfies the criteria given in (Imel, 1994) to use reference receivers less than 200km away for ionospheric corrections. A digital elevation map with one-meter horizontal resolution was provided by the United States Geological Survey (USGS) 3DEP LiDAR survey (U.S. Geological Survey, 2020) and processed in NASA's NavQ navigation risk assessment prognostic service (Gutierrez et al., 2024).

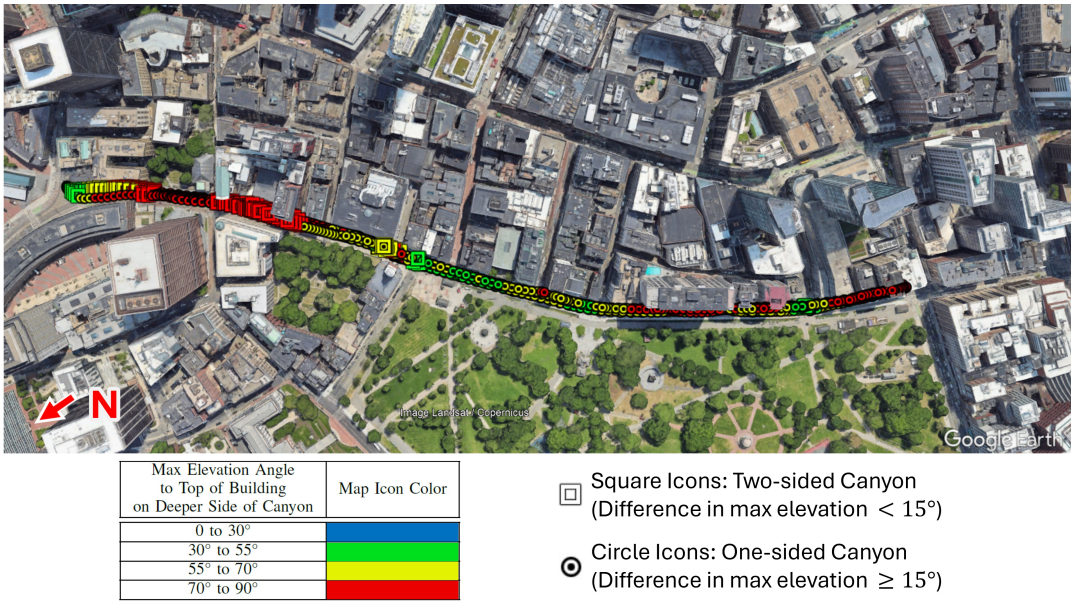

Figure 3: Overhead view of the receiver trajectory. The waypoints of the receiver trajectory are assigned colors and shapes according to their depth and "sidedness" features pictured. The thresholds for these features are chosen according to the prior work, (Peretic et al., 2025)

V. RESULTS

This section describes the analysis of the behavior of the pseudorange errors attributed to multipath and NLOS errors. Over the test trajectory, the u-Blox M8 generated 5984 measurements from LOS satellites and 7427 measurements from NLOS satellites, respectively. After the data was decimated, the Septentrio Mosaic generated 5748 LOS and 4631 NLOS measurements over the same trajectory. Figure 8 shows a time series of the count of LOS and NLOS measurements for the u-Blox M8 and Septentrio Mosaic, respectively. The two receivers performed comparably in generating measurements from the LOS satellites, but were notably different in generating measurements from the NLOS satellites.

While the u-Blox M8 and the Septentrio Mosaic share one antenna due to the data collection configuration, the Septentrio Mosaic also uses a second antenna. Dual-antenna receiver designs can perform additional multipath and NLOS reception detection tests, such as carrier-phase single differencing techniques (Santos and Farret, 2002), to aid in excluding NLOS pseudorange measurements from the navigation solution. The two receivers may also differ in design strategy, as well. Some receivers may aim to exclude NLOS measurements due to the errors they can introduce in the overall position solutions (Gilabert et al., 2023) and employ advanced tracking loop designs, such as (Siebert et al., 2023), and dedicated tests for multipath and NLOS reception, such as the well-known code-minus-carrier technique (Betz, 2015). However, these approaches may require additional computing resources, which may not be acceptable for certain use cases. Additionally, the NLOS measurements can offer useful information. When a receiver has few measurements available, using NLOS measurements may enable a receiver to solve for a navigation solution when there aren't a sufficient number of LOS satellites alone, potentially trading off some accuracy for increased availability. Techniques like direct position estimation (Ng and Gao, 2016) and vector tracking with knowledge of whether the signals are LOS or NLOS (Xu et al., 2020) may achieve better positioning accuracy with more NLOS measurements. Whether or not NLOS measurements are desirable to include is dependent on a) the application, b) whether those measurements are known to be NLOS, and c) whether the types of errors they introduce are modeled.

Figure 4 provides histograms of the errors in the pseudorange measurements due to multipath interference and NLOS effects for the two test receivers along the receiver's trajectory. Measurements are assigned a unique color and hatch pattern to identify their source satellite, as given in the legend. The letter "G" denotes that these are Global Positioning System (GPS) signals, and the number denotes the pseudorandom noise (PRN) code number of the measurement. The histogram bins are fixed to 2.5m for these and all subsequent plots. Table 1 provides metrics to describe these histograms. These data offer insights into which aspects of pseudorange error distributions are likely common across different receiver designs, and which aspects may differ.

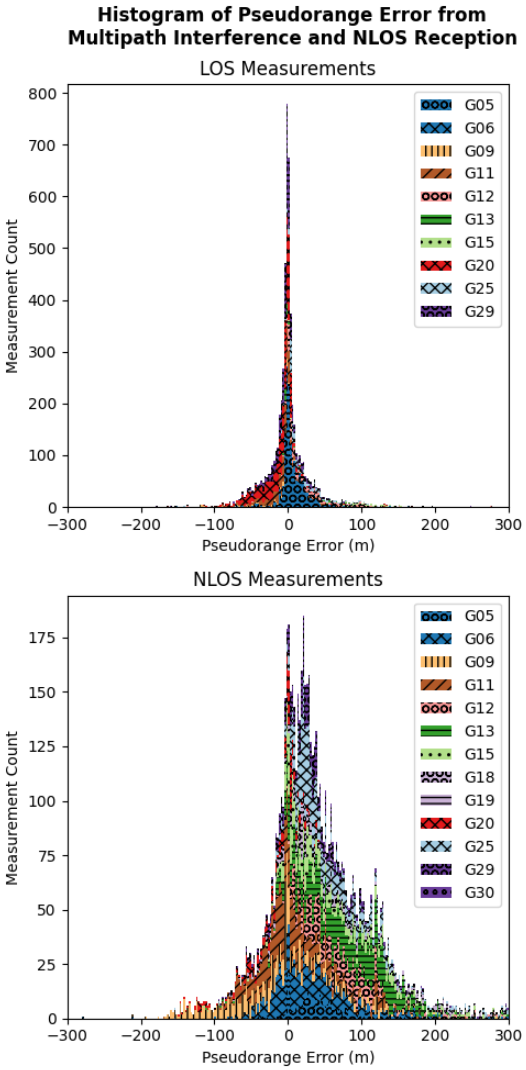

(a) Pseudorange errors in measurements from the u-Blox M8 receiver.

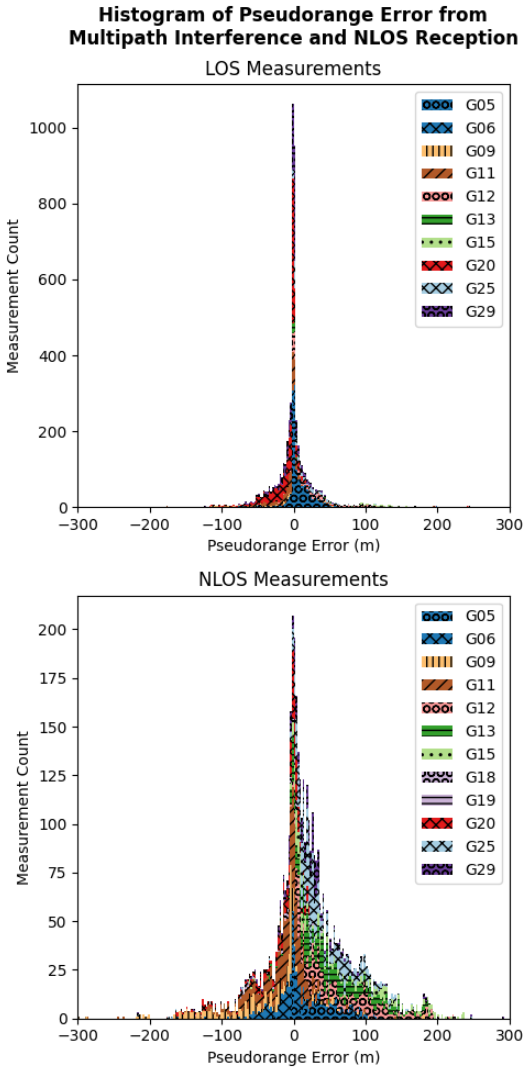

(b) Pseudorange errors in measurements from the Septentrio Mosaic receiver.

Figure 4: Histogram of pseudorange errors due to multipath interference and NLOS effects over the full data collection trajectory. Note the difference in y-axis scales for LOS vs. NLOS plots.

Table 1: Metrics characterizing the distribution of pseudorange errors due to multipath interference and NLOS effects.

Metric	u-Blox M8 LOS Measurements	Septentrio Mosaic LOS Measurements	u-Blox M8 NLOS Measurements	Septentrio Mosaic NLOS Measurements
Mean (m)	0.5	0.3	53.2	22.7
Median (m)	-0.6	-0.2	31.0	12.9
Errors between 25m and 125m (%)	11.4	10.1	41.6	32.6
Errors between -25m and -125m (%)	12.8	11.4	9.9	12.7
Errors between -25m and 25m (%)	75.1	78.0	34.0	47.0
Errors between 0m and 100m (%)	44.7	45.9	55.6	56.0

1. Overall Trends

The LOS measurements appear nearly symmetric for both the u-Blox M8 and the Septentrio Mosaic. Visually, the histograms appear nearly zero-mean and nearly symmetric in shape. Table 1 shows the mean and median values of the data from the two receivers. The receivers experience some difference in variance; the histograms for both receivers appear to have inflection points around $\pm$ 25m, but the majority of the mass in the tails of the errors from the u-Blox M8 appears to extend to roughly $\pm$ 80m, while the majority of the mass in the tails of the errors from the Septentrio Mosaic extend to roughly $\pm$ 50m. This is reflected in Table 1; the proportion of measurements within certain regions of the LOS histograms are within a few percentage points of each other, with the Septentrio Mosaic exhibiting a slightly tighter distribution.

The histograms formed from NLOS measurements also share some similarities. Both histograms have many measurements with near zero error. These measurements may be the result of situations such as a) diffraction enabling the signal to propagate over urban canyon edges to the receiver with minimal power loss and minimal additional delay, b) the signal propagating through trees lacking foliage or through glass (which the digital elevation map and measurement classification technique may treat as solid), or c) the receiver continuing to produce measurements of a recently-blocked signal when no NLOS reflections of sufficient power are present. The histograms have greater mass in the positive error direction, which is expected given that NLOS reflections will have a longer path length than the LOS path. Both histograms also have tails in the negative error direction, which can be due to multiple copies of NLOS reflections interfering with each other, or due to the aforementioned situations where the LOS signal is only marginally affected by blockage.

In contrast, the histograms formed from NLOS measurements have significant differences in the weight of tails, as shown in Figure 4. The Septentrio Mosaic has nine percent less of its mass in the 25m to 125m range compared to the u-Blox M8 receiver. Proportionally, more of this mass is shifted towards the center, as the Septentrio Mosiac has 13% more of the proportion of its measurements in the -25m to 25m range compared to the u-Blox M8. This leads to significantly different mean and median values in the two receivers' histograms, with the mean being 30m closer to zero and the median being 18m closer to zero for the Septentrio Mosaic than the u-Blox M8.

A factor in the difference between the receivers' error histograms may be the number of recorded measurements. The u-Blox M8 recorded 2796 more measurements of NLOS signals compared to the Septentrio Mosaic over the trajectory. In total, the u-Blox recorded 348 measurements more measurements with NLOS reception errors between -25m and 25m than the Septentrio, and 1580 more measurements with such pseudorange errors between 25m and 125m. This indicates that the weight of the tail is an aspect which can vary significantly between receivers. This may be the result of different receiver design decisions, such as in the number and spacing of tracking loop taps, different tracking lock detection criteria, or residual monitoring and outlier detection in the position solution phase.

However, it appears that neither of the histograms formed from NLOS measurements would be well-modeled by a Gaussian distribution. Both histograms exhibit heavy tails in the positive error direction for both receivers. Both share a very similar proportion of measurements in the 0m to 100m region (differing by less than one percent) and in the -25m to -125m region (differing by less than three percent). Relative to the other parts of the tails, both receivers have significantly fewer errors which are less than -150m or greater than 200m. So, although the mean, median, and the distribution of the weight in the tails can vary significantly across receivers, it may be reasonable to expect that urban canyon NLOS effects will cause distributions of errors with the majority of their mass near zero, a larger tail in the positive error direction, and possibly comparable limits for what may be considered outliers in the distribution.

2. Per-Satellite Trends

The histograms formed from LOS measurements in Figure 4 indicate that, despite the overall nearly zero-mean, nearly symmetric shape, the errors from individual satellites may not be. For example, the measurements from G05 and G20 exhibit tails in the positive and negative error directions, respectively. This behavior is consistent across both receivers. Further, this is not an artefact of the pseudorange error isolation methodology; the receivers' raw carrier phase measurements exhibit corresponding behaviors indicative of some fundamental underlying signal propagation effect.

Figure 5 examines one situation in the dataset where this effect is particularly distinct. This histogram plots pseudorange errors due to multipath interference and NLOS effects of only the measurements recorded during the second lap of the receiver trajectory for satellites G05 and G20 specifically. The overall shapes of the histograms for the LOS measurements' multipath errors still appear nearly zero-mean symmetric in shape. However, the measurement errors to G05 and G20 individually are clearly asymmetric, and are nearly mirror images of each other. Figure 6 shows time series plots of the rate of change of the receivers' raw carrier phase cycle counts, computed by differencing each measurement's reported carrier phase cycle count with the carrier phase cycle count from the previous second's observation. To aid comparison with Figure 5, the datapoints displayed in Figure 6 are only the carrier phase differences for which both the current second and the previous second produced carrier phase measurements from LOS satellites. For ease in comparing the curves to each other, the median datapoint of each timeseries has been subtracted from each time series.

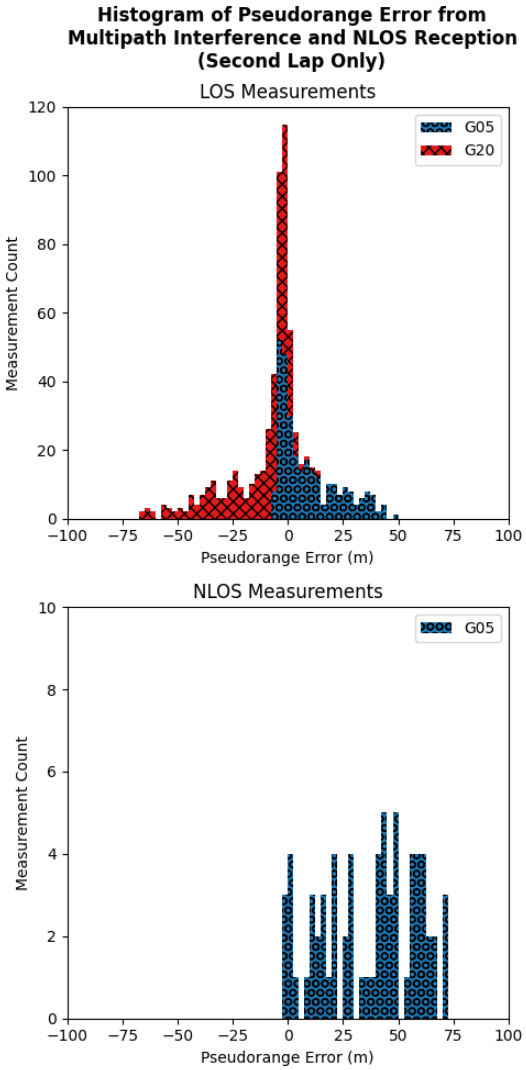

(a) Pseudorange errors in measurements from the u-Blox M8 receiver.

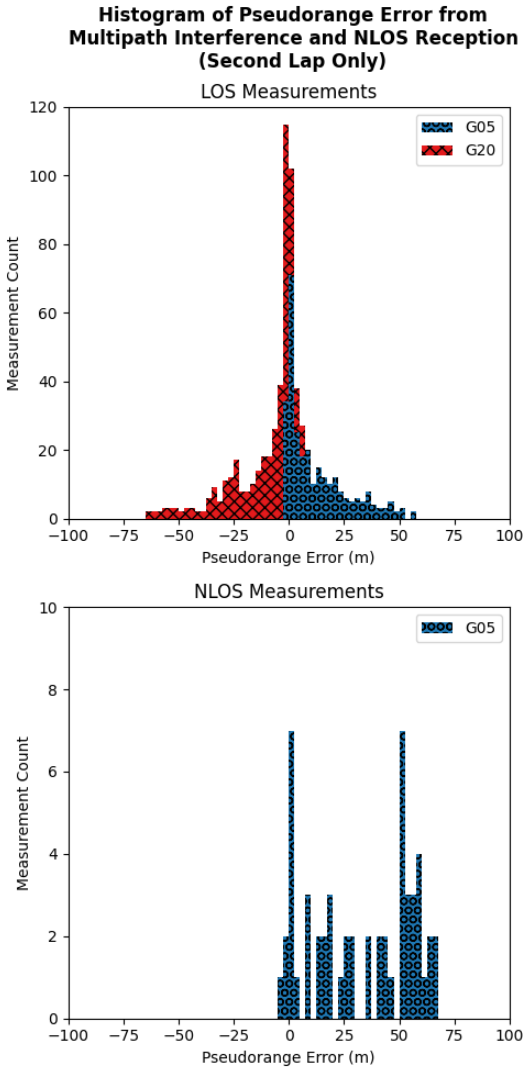

(b) Pseudorange errors in measurements from the Septentrio Mosaic receiver.

Figure 5: Histogram of pseudorange errors due to multipath interference and NLOS effects for measurements from the second lap of the receiver trajectory from satellites PRN 5 and 20. No measurements to satellite PRN 20 were classified NLOS over this interval of the trajectory.

Figure 6 show three regions where the carrier phase rate of change for the two satellites temporarily changes in a manner visually similar in scale and shape, but opposite in direction. This implies that the difference in the pseudorange measurements for PRNs 5 and 20 temporarily increases, then decreases back to roughly the previous difference. The pseudorange errors within the orange areas of Figure 6 are separated and plotted as histograms in Figure 9. Again, the mirror-image relationship between G05 and G20 is evident.

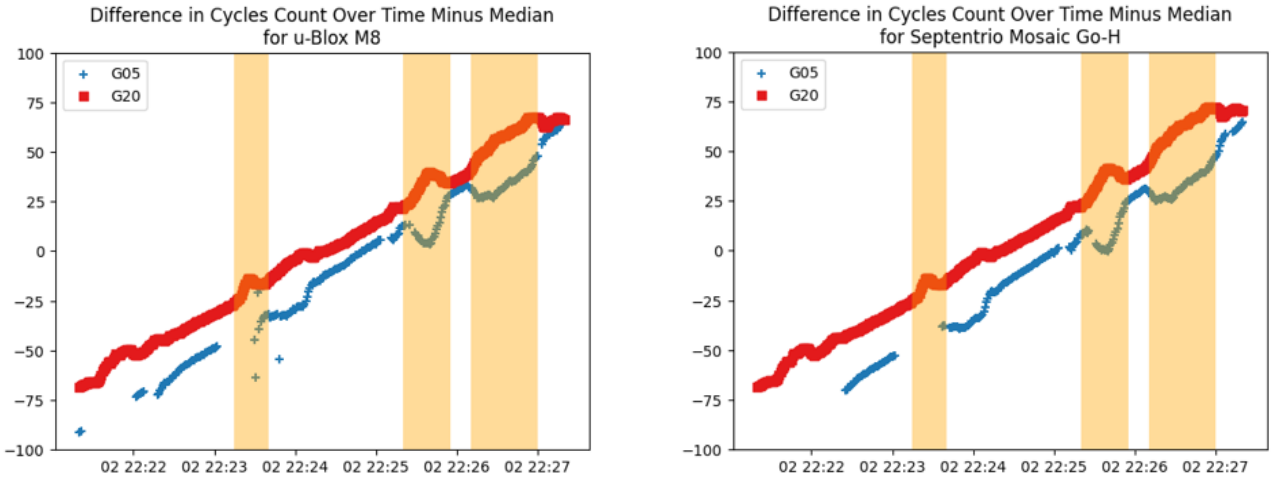

(a) Measurements from the u-Blox M8 receiver.

(b) Measurements from the Septentrio Mosaic receiver.

Figure 6: Change in carrier phase measurements over time for LOS measurements from satellites PRN 5 and 20 along the second lap of the receiver trajectory. The median value has been subtracted from the time series to bring the curves near to each other for comparison purposes.

This behavior persists across other satellites and other laps in the receiver trajectory; for brevity, only the case of PRN 5 and 20 in the second lap of the receiver trajectory is discussed here.

VI. CONCLUSION

This paper presented the statistical behavior of pseudorange errors multipath interference and NLOS reception in two commercial receivers in an urban canyon environment. The histograms of multipath errors on LOS measurements were nearly zero-mean and nearly-symmetric both receivers. For the known-NLOS measurements, both receivers showed a distribution of errors with greater mass in the positive error direction, and the distributions were largely contained within the -150m to 200m range. However, the amount of mass in the tails of the distributions differed between the two receivers, changing certain statistical metrics like the mean and median. This paper also presented the behavior of multipath errors from LOS measurements to two specific satellites during one particular segment of the dataset. In this segment, the two satellites manifested as asymmetric, tailed distributions of errors, which were near-mirror images of each other.

Access to the receiver internals is likely necessary to further analyze the cause of such behavior in the distribution of the pseudorange errors. As analytically modeled by the multipath error envelope concept, differences in tracking loop tap spacing and the discriminator equation can lead to tens of meters of difference in the maximum possible pseudorange error under a given multipath or NLOS reception effect. Future work may include studying more GNSS receivers and how the pseudorange errors of these receivers vary as a function of urban canyon features. A software-defined receiver post-processing a digitized recording of raw radio frequency measurements from a given urban environment would enable study of how specific receiver design parameters affect pseudorange error in urban environments. Additionally, comparing the pseudorange error performance of multiple receivers (various fixed commercial implementations and/or various configurations of software-defined implementations) as a function of urban canyon features could inform trade-offs in receiver design. For example, two receivers may perform similarly in canyons with a certain combination of features, and perform differently in canyons with a different set of features. Such trade-offs may be useful in mission planning; for example, a lower-cost receiver may be an appropriate choice for a mission if that mission is known to only exhibit certain types of canyon features, and if it is known that the lower-cost receiver performs sufficiently with respect to those specific features.

These results also offer new insights to urban GNSS integrity and resilient receiver architectures. Since the seminal work on Gaussian overbounding for GNSS receiver integrity described in (DeCleene, 2000), such overbounding techniques have been studied to conduct pseudorange integrity analysis without requiring that the data hold to a zero-mean Gaussian assumption. Finding methods to tightly overbound non-zero mean long-tailed distributions, particularly if the methods can tightly overbound to the variation in mass in the tail shown in this work, would offer new tools in urban navigation risk assessment. Additionally, the aforementioned trends in the histograms presented in this work could offer insights into receiver architectures which could compensate for these pseudorange error effects. To improve multipath and NLOS rejection, topics like tracking loop tap counts and spacing, tracking lock criteria, and carrier phase analysis informed by these results could lead to improved navigation

performance. In contrast, to incorporate multipath-affected and NLOS pseudorange measurements in a manner that improves navigation performance, vector tracking algorithms which detect NLOS measurements and Kalman filter variants which model long-tailed distributions could be fruitful areas of study.

ACKNOWLEDGMENT

The authors thank Jared Shalke (MITRE) for his technical support in collecting the data studied in this work, as well as Dr. Esther Conrad (NASA), Dr. Sarah Lehman (NASA), and Dr. Sharon Marroquin (MITRE) for their technical review of the manuscript.

REFERENCES

Betz, J. W. (2015). *Engineering Satellite-Based Navigation and Timing*. John Wiley & Sons, Ltd.

Chen, X. (2018). Statistical multipath model comparative analysis of different GNSS orbits in static urban canyon environment. *Advances in Space Research*, 62(5):1034–1048.

DeCleene, B. (2000). Defining pseudorange integrity - overbounding. In *Proceedings of the 13th International Technical Meeting of the Satellite Division of The Institute of Navigation (ION GPS 2000)*, pages 1916–1924, Salt Lake City, UT.

Dill, E., Gutierrez, J., Young, S., Moore, A., Scholz, A., Bates, E., Schmitt, K., and Doughty, J. (2021). A predictive GNSS performance monitor for autonomous air vehicles in urban environments. In *Proceedings of the 34th International Technical Meeting of the Satellite Division of The Institute of Navigation (ION GNSS+ 2021)*, pages 125–137, St. Louis, Missouri.

Gilabert, R., Gutierrez, J., and Dill, E. (2023). Improvements to GNSS positioning in challenging environments by 3DMA lidar informed selective satellites usage. In *Proceedings of the 36th International Technical Meeting of the Satellite Division of The Institute of Navigation (ION GNSS+ 2023)*, pages 2606–2615, Denver, Colorado.

Gutierrez, J., Young, S., Moore, A., Gilabert, R., Dill, E., Bates, E., Peretic, M., Schmitt, K., and Scholz, A. (2024). A High-Performance Computing Predictive GNSS Performance Monitor for Autonomous Air Vehicles in Urban Environments. Technical Report 20240009932, NASA Langley Research Center, Hampton, VA.

Imel, D. A. (1994). Evaluation of the TOPEX/POSEIDON dual-frequency ionosphere correction. *Journal of Geophysical Research: Oceans*, 99(C12):24895–24906.

Matera, E. R., Garcia-Pena, A., Julien, O., Milner, C., and Ekambi, B. (2019). Characterization of line-of-sight and non-line-of-sight pseudorange multipath errors in urban environment for GPS and Galileo. In *Proceedings of the 2019 International Technical Meeting of The Institute of Navigation*, pages 177–196, Reston, Virginia.

McGraw, G. A., Groves, P. D., and Ashman, B. W. (2021). Robust positioning in the presence of multipath and NLOS GNSS signals. In *Position, Navigation, and Timing Technologies in the 21st Century: Integrated Satellite Navigation, Sensor Systems, and Civil Applications*, pages 551–589.

Ng, Y. and Gao, G. X. (2016). Direct position estimation utilizing non-line-of-sight (NLOS) GPS signals. In *Proceedings of the 29th International Technical Meeting of the Satellite Division of The Institute of Navigation (ION GNSS+ 2016)*, pages 1279–1284, Portland, Oregon.

Patterson, M., Isaacson, D., Mendonca, N., Neogi, N., Goodrich, K., Metcalfe, M., Bastedo, B., Metts, C., Hill, B., DeCarme, D., Griffin, C., and Wiggins, S. (2021). An initial concept for intermediate-state, passenger-carrying urban air mobility operations.

Peretic, M., Gilabert, R., Carroll, J., Gutierrez, J., Moore, A., Christie, J., and Dill, E. (2025). Statistical analysis of GNSS multipath errors in urban canyons. In *2025 IEEE/ION Position, Location and Navigation Symposium (PLANS)*, pages 1216–1225, Salt Lake City, Utah.

Santos, M. C. and Farret, J. C. (2002). Analysis and generalization of a dual-antenna multipath mitigation technique. In *Proceedings of the 15th International Technical Meeting of the Satellite Division of The Institute of Navigation (ION GPS 2002)*, pages 287–288, Portland, OR.

Siebert, C., Konovaltsev, A., and Meurer, M. (2023). Development and validation of a multipath mitigation technique using multi-correlator structures. *NAVIGATION: Journal of the Institute of Navigation*, 70(4).

U.S. Geological Survey (2020). USGS Lidar Point Cloud MA_CentralEastern_1_2021. https://apps.nationalmap.gov/lidar-explorer/. Accessed: 2020-02-23.

Wang, Y., Chen, X., and Liu, P. (2018). Statistical multipath model based on experimental GNSS data in static urban canyon environment. *Sensors*, 18(4).

Xu, B., Jia, Q., and Hsu, L.-T. (2020). Vector tracking loop-based GNSS NLOS detection and correction: Algorithm design and performance analysis. *IEEE Transactions on Instrumentation and Measurement*, 69(7):4604–4619.

Zhu, N., Marais, J., Bétaille, D., and Berbineau, M. (2018). GNSS position integrity in urban environments: A review of literature. *IEEE Transactions on Intelligent Transportation Systems*, 19(9):2766–2779.

A. SUPPLEMENTAL FIGURES

This section includes additional figures to supplement the analysis in Section V.

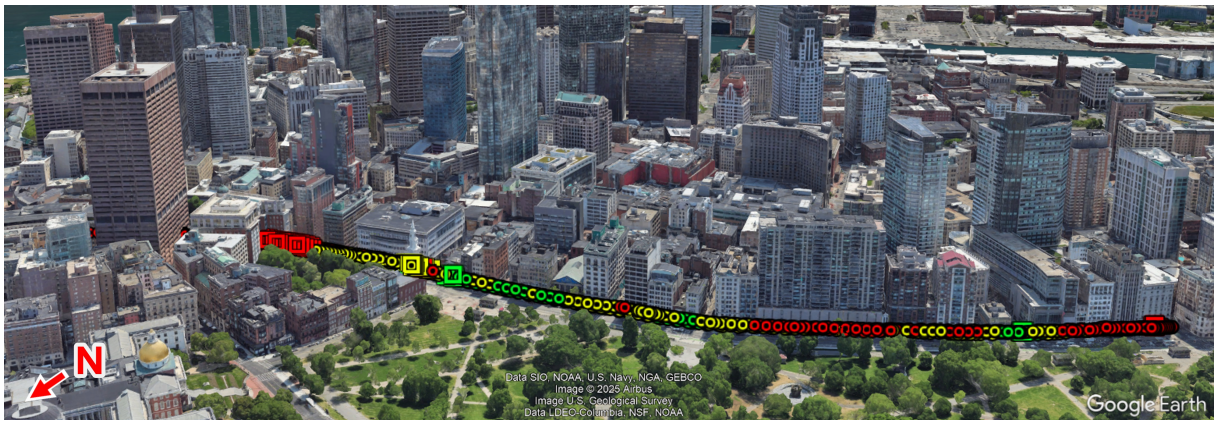

(a) Isometric view of receiver trajectory

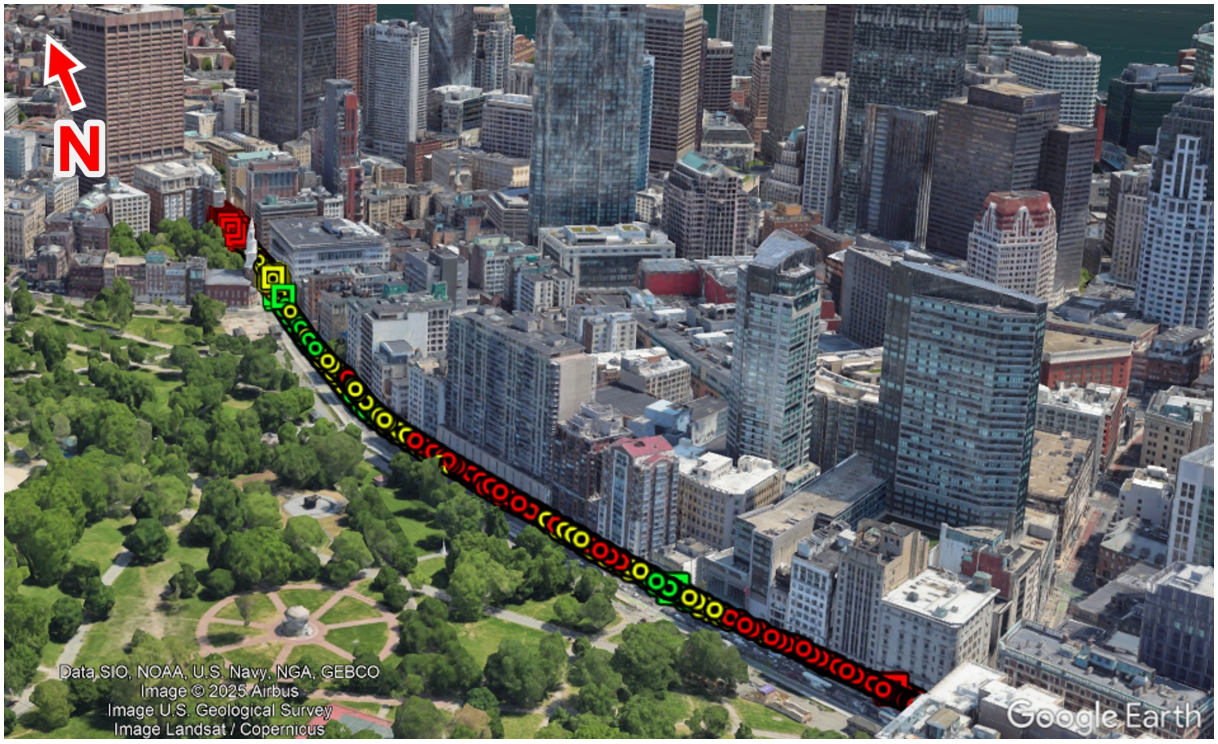

(b) View of receiver trajectory along the canyon

Figure 7: Supplemental views of the receiver trajectory. Waypoint color and shape is consistent with the legend provided in Figure 3.

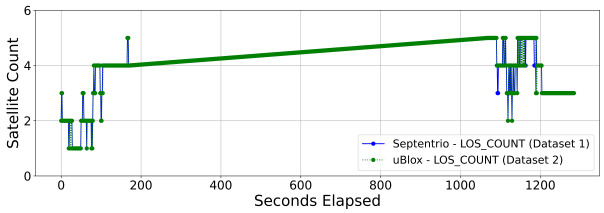

(a) First lap LOS counts. The vehicle was stationary for roughly 15 minutes, and measurements from that portion of the trajectory have been excised for consistency with the other laps.

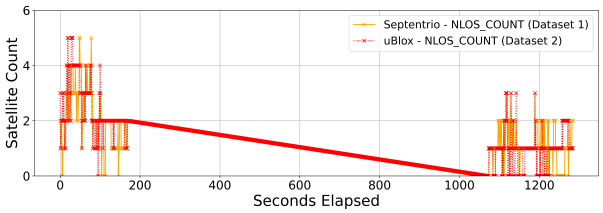

(b) First lap NLOS measurement counts. The vehicle was stationary for roughly 15 minutes, and measurements from that portion of the trajectory have been excised for consistency with the other laps.

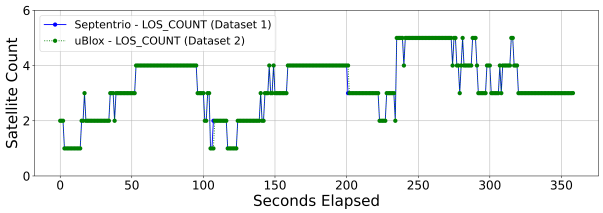

(c) Second lap LOS measurement counts

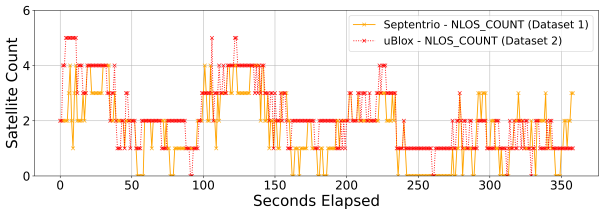

(d) Second lap NLOS measurement counts

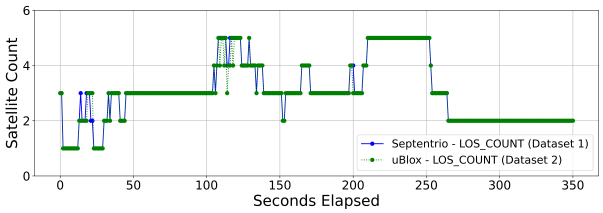

(e) Third lap LOS measurement counts

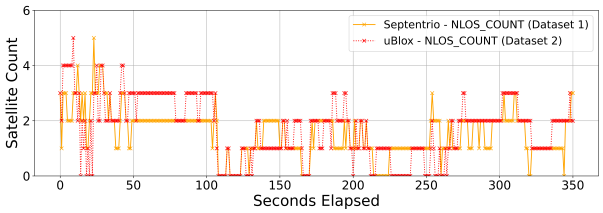

(f) Third lap NLOS measurement counts

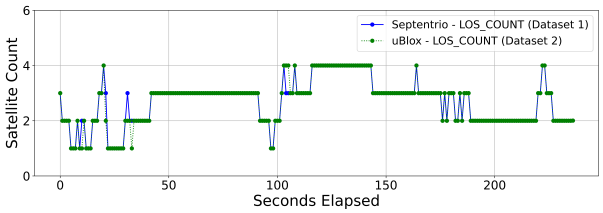

(g) Fourth lap LOS measurement counts

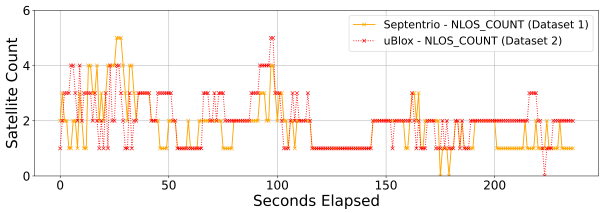

(h) Fourth lap NLOS measurement counts

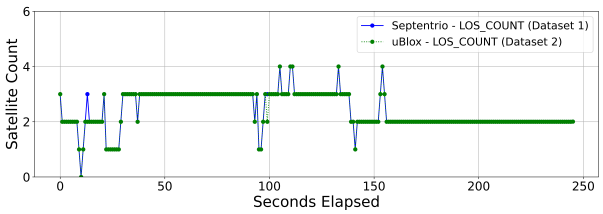

(i) Fifth lap LOS measurement counts

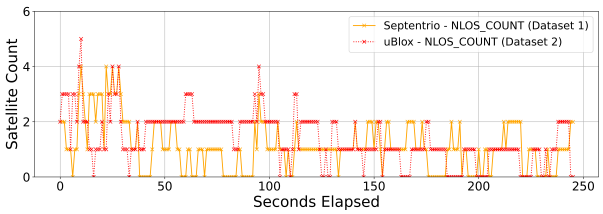

(j) Fifth lap NLOS measurement counts

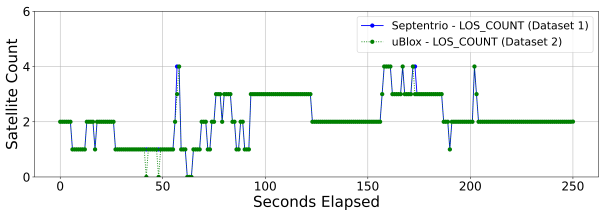

(k) Sixth lap LOS measurement counts

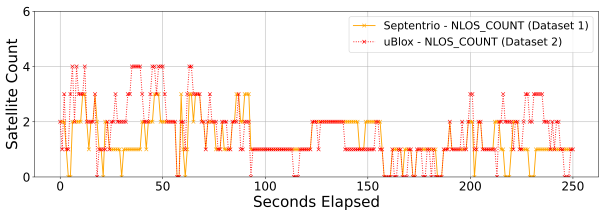

(l) Sixth lap NLOS measurement counts

Figure 8: Number of measurements recorded by the two test receivers over the dataset.

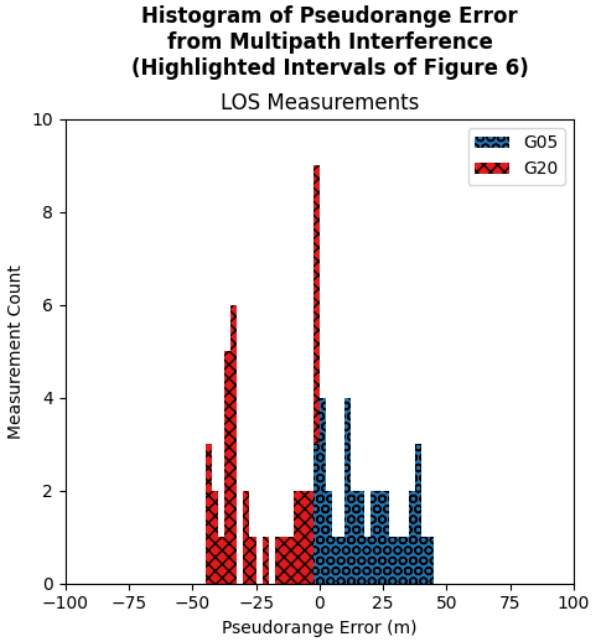

(a) Pseudorange errors in measurements from the u-Blox M8 receiver.

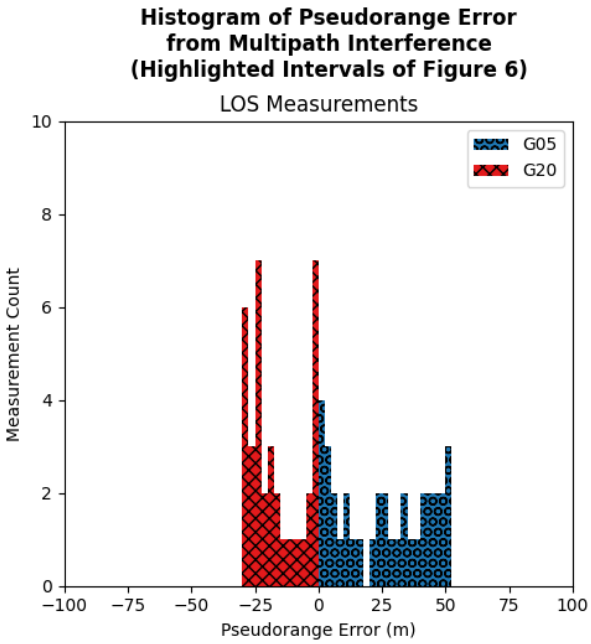

(b) Pseudorange errors in measurements from the Septentrio Mosaic receiver.

Figure 9: Statistical distribution of pseudorange errors due to multipath interference for measurements from the orange regions of Figure 6 in the second lap of the receiver trajectory from satellites PRN 5 and 20.